Determining the detection efficiency and background level of ATIC electron observation from flight data

J. Chang*, J. Wu*, T. G. Guzik†, J. P. Wefel†, J. Isbert†, J. H. Adams, Jr.‡, M. Christl‡, J. Watts‡, H. S. Ahn§, K.C. Kim§, E. S. Seo§, J. Wu§, G. L. Bashindzhagyan¶, E. N. Kouznetsov¶, M. I. Panasyuk¶, N. V. Sokolskaya¶, A. D. Panov¶, and V. I. Zatsepin¶

*Purple Mountain Observatory, Chinese Academy of Sciences, China
†Louisiana State University, Department of Physics and Astronomy, Baton Rouge, LA, USA
‡Marshall Space Flight Center, Huntsville, AL, USA
§University of Maryland, Institute for Physical Science & Technology, College Park, MD, USA
¶Skobeltsyn Institute of Nuclear Physics, Moscow State University, Moscow, Russia

Abstract. **Observations of Cosmic-ray electrons are difficult due to the large flux of cosmic ray hadrons. The event selection efficiency and background levels can be estimated from flight data for the ATIC instrument. This reduces the dependence upon Monte Carlo simulations, which show differences between different codes, thereby reducing the systematic errors resulting from analyses that only use simulations. This paper discusses some of the methods used in the ATIC analysis to determine the detection efficiency and background level for the flight data.**

Keywords**: ATIC; high energy electron; high energy gamma-ray**

I. Introduction

The ATIC (Advanced Thin Ionization Calorimeter) balloon experiment is a calorimeter based instrument developed to study the spectra of cosmic ray nuclei to the highest energies allowed by the exposure (near 100 TeV for protons) [1]. It is also possible for ATIC to measure very high energy electrons [2], [3] using a technique we developed [3] that involves details of the shower development in the instrument. The first results from this analysis for the ATIC-1 and ATIC-2 Antarctic balloon flights have been published [4] .

The ATIC instrument consists of a fully active calorimeter with 2.5cm X 2.5cm X 25cm BGO logs arranged in orthogonal layers (8 layers in ATIC-1,2 and 10 layers in ATIC-4) which capture about 85% (ATIC-1,2) or 93% (ATIC-4) of the energy in the electromagnetic cascades. The calorimeter is located under a 30 cm thick carbon target containing (top, center, bottom) three layers of crossed scintillator strip hodoscopes (S1, S2, S3) to provide both the fast trigger and tracking. At the top is a pixilated Silicon matrix detector to measure the charge of the incident particle with minimum effect from the backscattered particles in the cascade. The instrument was calibrated with beams of both protons and electrons from the CERN SPS [5], and these data provide a calibration/normalization for the analysis.

The main problem for a calorimeter based analysis is to separate the electron signal from the proton background and to determine the unresolved proton background that may still remain within the electron dataset. There are two complementary approaches to determining the event selection efficiency and the background level – Simulation codes and In-flight data. Elsewhere at this conference analysis of the ATIC data using only simulations are discussed [6]. Unfortunately, simulations of shower development can be quite different for different codes [6], [7], as well as different from the experimental data. In [7], it was shown the different codes, especially GEANT3.21, could not reproduce the shower lateral development. So, if electron selection is based only on simulation, systematic errors may be introduced. Here we discuss analysis of the ATIC using in-flight data.

II. Electron event selection in ATIC

As a balloon instrument, ATIC observes both electrons and atmospheric secondary gamma-rays at the same time. A typical gamma-ray event passes first through the charge module (Silicon matrix plus S1), then initiates its electromagnetic cascade in the target and completes the shower development in the BGO calorimeter. Backscatter from the shower completes the trigger for such events. The charge module is used as an anticoincidence system in off-line analysis. Since backscattering from the shower is almost isotropic, several scintillator strips around the incident trajectory can be used as the anticoincidence. The number of strips is determined by the trajectory resolution, detection efficiency and background level depend on the number of strips. The primary trajectory is determined from the cascade core, as measured by the crossed (x,y) BGO crystals and plastic scintillators in the carbon target. From the calculated energy deposit distribution in each BGO layer, the position of the maximum energy deposit of the cascade core is determined. The event trajectory,

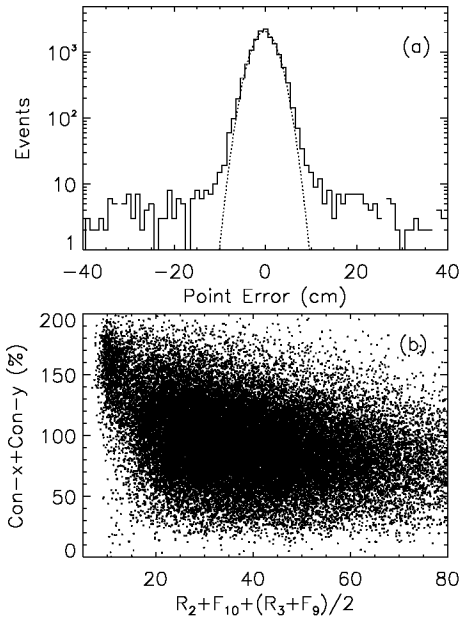

Fig. 1. (a):positional resolution in the X-Z plane for singly charged events with energy deposit in BGO above 50 GeV, (b): distribution of Con-x + Con-y plotted versus the shower selection parameters .

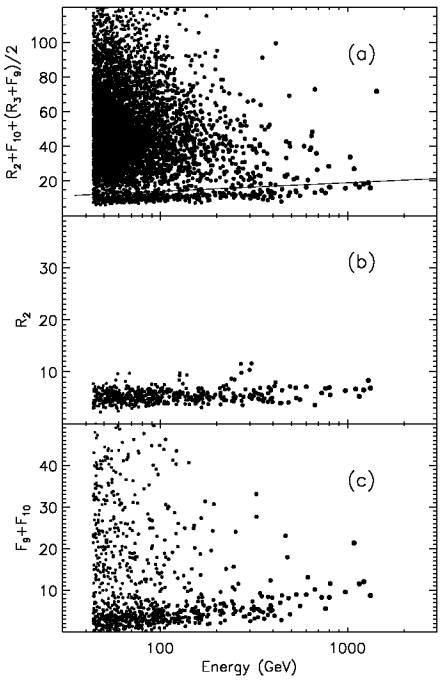

Fig. 2. The energy dependence of the gamma ray shower parameters (see text for details).

so determined, is used to predict the hit position in the charge module.

Figure 1 (top) shows positional resolution in the X-Z plane for singly charged events with energy deposit in the BGO above 50 GeV. The position is the distance between the calculated hit position and the nearest particle hit in the charge module. The top solid line shows all events, and this distribution has wide wings compared to the (dashed) Gaussian fit. Such wing events are Gamma-ray like events. If we use 5 strips around the shower axis (total 10 cm) as an anticoincidence, we obtain mostly gamma-ray events, with only a small proton background.

The gamma-ray events are easily distinguished from the small proton background, and, since gamma-ray showers are essentially identical to electron showers, these secondary gammas can be used as a template for selecting electrons from their (more numerous) proton background. Simulations are also employed to cross-check the event selection criteria derived from the gamma-ray events.

The first step in separating electrons from the proton background makes use of the shower starting point distribution which is different for electrons and protons. If the proton interaction point is in the carbon target, in general, many secondary particles are produced and these spread around the shower axis. By analyzing the shower energy center in scintillator S3 at the bottom of the target section, this difference is utilized as part of the proton background rejection. Defining the shower energy center by Con-x (in S3X)=(energy deposit around shower axis)/Total energy deposit in S3X, plus the equivalent for the y direction, Figure 1 (bottom) shows the distribution of Con-x + Con-y plotted versus the shower selection parameters. Electron-like events cluster in the upper left of this plot, and a suitable cut rejects about 70% of the protons.

We then define two parameters to describe the shower development in the ATIC calorimeter:

$$R_i^2 = \frac{\sum_{i=1}^{n} E_i (x_i - x_c)^2}{\sum_{i=1}^{n} E_i} \quad (1)$$

$$F_j = R_j^2 [E_j / \sum_{i=1}^{n} E_i] \quad (2)$$

where R_i is the shower width and F_j is the energy fraction weighted by the square of the shower width, where i (j) refers to the layer of the calorimeter. In Figure 1(bottom), the $R_2+F_{10}+(R_3+F_9)/2$ distribution clearly depends on energy.

Next, we find the Gamma-like events by hit analysis around the shower axis, as described previously. Figure 2(a) shows the $R_2+F_{10}+(R_3+F_9)/2$ energy dependence for all gamma-ray like events. The gamma-ray signal is very clear, especially at high energy where the gammas are almost background free. Setting a loose cut such as the dashed line in Figure 2(a), we then look at the R_2

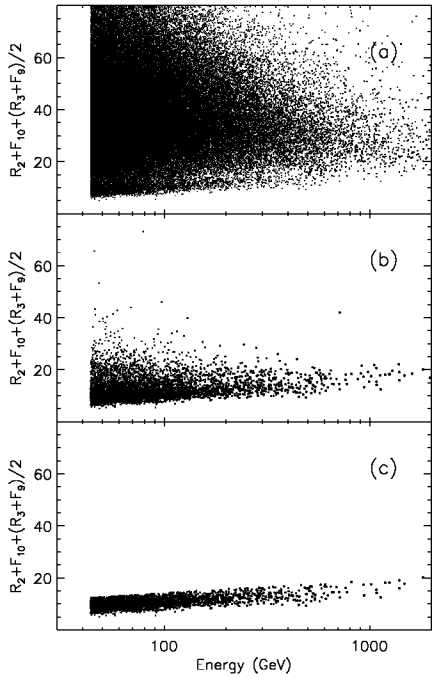

Fig. 3. The steps in electron selection in the ATIC data, as described in the text.

distribution,Fig.2(b), and observe that it is essentially background free. From simulation studies, R_2 can be shown to be essentially independent of energy. Thus, Fig 2(b) defines the cut to be applied for electron event selection by theR_2 parameter. Now, Figure 2(c) shows the $F_9+ F_{10}$ distribution after R_2 cut and its dependence on energy for all gamma-ray like events (90% of the proton background has been rejected). Since the gamma-ray signal is very clear, the $F_9+ F_{10}$ distribution, in different energy ranges, provides the $F_9+ F_{10}$ cut (energy dependent) to be used for electron selection.

This analysis procedure, with cut parameters determined from the gamma-ray analysis, is applied to the electron-like events as shown in Fig.3, where Fig.3(a) is identical to Fig.2(a), but showing all electron-like events. Figure 3(b), after the $F_9+ F_{10}$ cut, shows more than 98% proton background rejection. Figure 3(c) after R_2 cut is the 'electron dataset'.

III. Background Determination

Within the 'electron dataset' there are three primary sources of background: unresolved proton events, secondary atmospheric) electrons, and mis-identified secondary gamma-rays. On average, the background is composed of 62% unresolved protons, 23% secondary atmospheric electrons and 15% mis-identified gamma-rays.

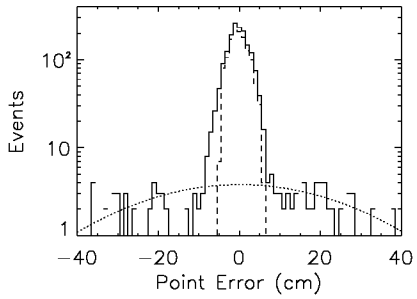

Fig. 4. Gamma-ray background calculation from positional resolution in the X-Z plane for all gamma-ray and electron like events with energy deposit in BGO above 100 GeV

A. Gamma-ray background

For some high energy secondary gamma rays, it is possible that the track of a backscattered particle is close to the incident gamma-ray trajectory, and such gamma-rays will mimic electrons. In Fig.4, solid histogram is for all gamma-ray and electron like events with energy deposit in BGO above 100 GeV. Dashed histogram is after electron event selection, and as in Fig.1, the 'wings' on the solid histogram is due to backscatter from gamma-ray events. Since backscatter from the shower in the calorimeter is almost isotropic, we use a simple function to estimate the point error distribution for gamma-ray like events. For an istropic distribution of backscatter, the background rate is about 2.1%. However if we assume the backscatter is more concentrated around the shower axis (e.g. the dotted gaussian distribution in Fig.4) the background rate is about 3.1%. From simulations for an isotropic distribution, the background rate is 2.0±0.1%, in agreement with the estimate from the flight data. Since the higher energy gamma-rays will produce more backscatter, the background rate changes with energy from 2% at 100 GeV to 3.6% at 1 TeV, with a systematic uncertainty on these numbers of below 10%.

B. Secondary electron background

Atmospheric secondary electron production has been analyzed in detail [8], and depends strongly on the cosmic-ray spectrum, including protons and heavy ions, whose contribution is about 52% of protons [9]. Using the flight altitude for the experiments, and following the previous work, we find for ATIC2 that the total secondary electron flux at the instrument is $2.1\pm0.2E^{-2.75}/(m^2$ sr sec.).

C. Proton background

We estimate the background rate from unresolved protons by analyzing the charge distribution before and after event selection, and by using the CERN beam test

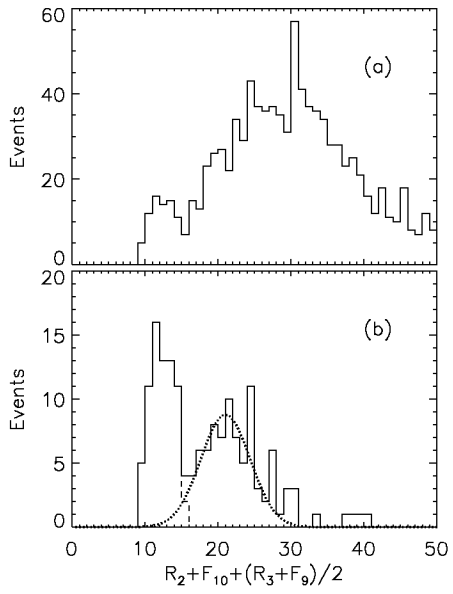

Fig. 5. Proton background estimation, detail can found in the text

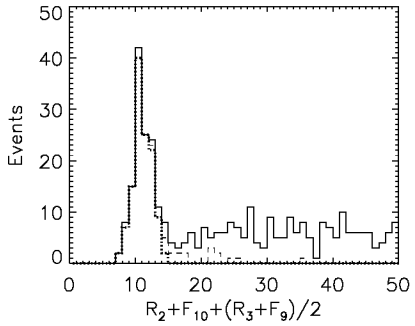

Fig. 6. Detection efficiency calculation by gamma ray-like events, detail can found in the text

data [3].

However, we can also obtain the background rate from flight data by using the gamma-rays as a 'ruler', since the gamma-ray signal is much less contaminated by protons than the electron signal. Looking at the density contours on a scatter plot for gamma-rays in a specific energy interval, the unresolved proton contribution can be estimated rather accurately, to within statistical limitations. This same fraction should also apply to the electron peak in the same energy interval.

For example, Fig. 5(a) shows the electron-like events between 350 GeV to 500 GeV. Fig.5(a) corresponds to the data in Fig.3(a) between 350 GeV to 500 GeV. In Fig.5(b) the solid histogram is after R_2 cut by gamma-ray, dashed histogram is after F_9+F_{10} cut. A distribution fit to the residual (dotted curve in Fig.5(b)) allows us to estimate corresponding proton background rate of 3.6±1.5%.

IV. Event Selection Efficiency Estimation for Gamma-Ray Events

Figure 6 shows all the gamma-ray-like events above 100 GeV, and the dashed histogram is after R_2 cut, dotted histogram is after F_9+F_{10} cut. It can be seen that the gamma-ray signal is almost background free, by analyzing the gamma-ray distribution before/after event selection, we obtain a gamma-ray event selection efficiency of 89.7±1.4%.

Because gamma-ray shower is almost identical with electrons, the gamma-ray event selection efficiency can be applied to electron data analysis.

V. Summary

We conclude that the use of the secondary gamma-rays provided by the residual atmosphere above the balloon provides an in-flight calibration method for the analysis of the electron data in ATIC to beyond the energy range of the previously reported excess. This method of analysis is less dependent upon simulations and less prone to the introduction of systematic uncertainties. At each step in the analysis there is substantial agreement between the experimentally determined parameters and the results of the simulations, but the exact parameters to be used are determined from the flight data whenever possible.

References

[1] T. G. Guzik, J.H. Adams Jr, H.S. Ahn et al. Adv. Sp. Res., V.33 (2004), P.1763.
[2] J. Chang, J. H. Adams Jr, H. S. Ahn et al. Proc. 28th ICRC (Tsukuba), 1817-1820, (2003) ;
[3] J. Chang, J.H. Adams Jr, H.S. Ahn et al. Adv. Sp. Res., V.42 (2008) P.431.;
[4] J. Chang, J. H. Adams Jr, H. S. Ahn et al. Nature, V.456 (2008) , P.362–365 .;
[5] O. Ganel, J.H. Adams Jr,, H.S. Ahn, et al. Nucl. Instr. Meth. V.A552 (2005), P.409.
[6] R. Xu, J. Chang, S. Torii et al. ChJAA. Vol 7, Issue 6, (2007), P.839.
[7] A. D. Panov, this conference (2009).
[8] J. Nishimura, et al.; ApJ. 238 (1980), 394
[9] M. Mori, ApJ, 478 (1997), 225